Electronic Origin for the Phase Transition from Amorphous Li_xSi to Crystalline $Li_{15}Si_4$

Meng Gu,[†] Zhiguo Wang,[‡,§] Justin G. Connell,[⊥] Daniel E. Perea,[†] Lincoln J. Lauhon,[⊥] Fei Gao,[‡] and Chongmin Wang[†,*]

[†]Environmental Molecular Sciences Laboratory and [‡]Fundamental and Computational Science Directorate, Pacific Northwest National Laboratory, Richland, Washington 99352, United States, [§]Department of Applied Physics, University of Electronic Science and Technology of China, Chengdu, 610054, People's Republic of China, and [⊥]Materials Science and Engineering, Northwestern University, Evanston, Illinois 60208, United States

ABSTRACT Silicon has been widely explored as an anode material for lithium ion battery. Upon lithiation, silicon transforms to amorphous Li_xSi (a-Li_xSi) *via* electrochemical-driven solid-state amorphization. With increasing lithium concentration, a-Li_xSi transforms to crystalline $Li_{15}Si_4$ (c-$Li_{15}Si_4$). The mechanism of this crystallization process is not known. In this paper, we report the fundamental characteristics of the phase transition of a-Li_xSi to c-$Li_{15}Si_4$ using *in situ* scanning transmission electron microscopy, electron energy loss spectroscopy, and density function theory (DFT) calculation. We find that when the lithium concentration in a-Li_xSi reaches a critical value of $x = 3.75$, the a-$Li_{3.75}Si$ spontaneously and congruently transforms to c-$Li_{15}Si_4$ by a process that is solely controlled by the lithium concentration in the a-Li_xSi, involving neither large-scale atomic migration nor phase separation. DFT calculations indicate that c-$Li_{15}Si_4$ formation is favored over other possible crystalline phases due to the similarity in electronic structure with a-$Li_{3.75}Si$.

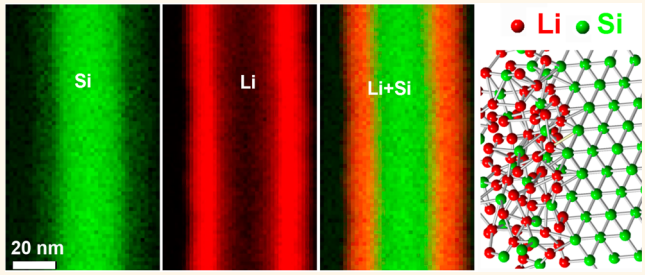

KEYWORDS: Si · lithiation · *in situ* TEM · EELS · phase transition · electronic structure

Silicon, as a candidate anode material for rechargeable lithium ion batteries, shows several unique characteristics. It has a theoretical gravimetric capacity of ~4200 mAh g^{-1} and a volumetric capacity of ~8500 mAh cm^{-3}. Upon lithiation, both crystalline and amorphous silicon transform to amorphous Li_xSi (a-Li_xSi), a process termed electrochemical-driven solid-state amorphization.[1] With continued Li enrichment, the a-Li_xSi subsequently crystallizes to a crystalline (Li, Si) compound. Accompanying the electrochemical-driven solid-state amorphization of silicon is a volume expansion of more than 300%, with dramatic anisotropic elongation along the [110] direction for the case of crystalline silicon.[2−5] The large volume change normally leads to the pulverization of the material. Both the large volume change and the phase transformation critically affect performance of the battery when silicon is used as an anode. The extent of volume change can be minimized by the design and synthesis of nanostructures to limit. A range of nanostructures have been investigated, including Si nanowires, nanotubes, nanoparticles of both crystalline and amorphous structures,[6−15] and silicon and carbon composite.[9,12,16−26]

Numerous experimental and theoretical studies have explored the phase and phase transformation characteristics of the Si−Li system.[27−32] Thermodynamically, crystalline intermetallics of Li and Si have much lower Gibbs energy than the amorphous alloys. As shown in a Li−Si phase diagram generated by heat treatment of a mixture of Li and Si (Figure 1),[33,34] a range of solid crystalline compounds can be formed including LiSi, $Li_{12}Si_7$, $Li_{13}Si_4$, and $Li_{22}Si_5$.[35] However, these crystalline (Li, Si) compounds do not form directly during the electrochemical-driven alloying of Si with Li,[1] despite the fact that the formation energies of crystalline (Li, Si) compounds are lower than those of the corresponding amorphous phases, as illustrated in Figure 2, based on density functional theory (DFT) calculation.[25] The phase transitions of a-Li_xSi alloys during Li insertion have been investigated by scanning

* Address correspondence to chongmin.wang@pnnl.gov.

Received for review May 10, 2013 and accepted June 24, 2013.

Published online June 24, 2013
10.1021/nn402349j

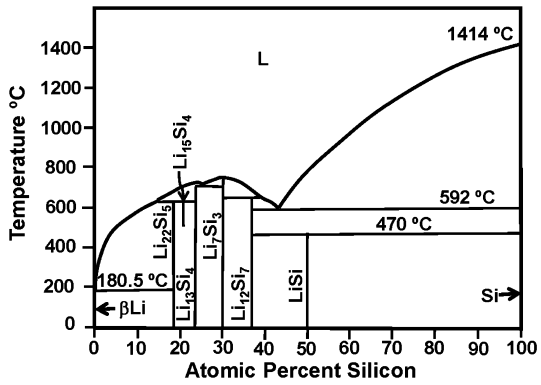

Figure 1. Phase diagram of the Li–Si system. Redrawn based on the figure published in ref 34.

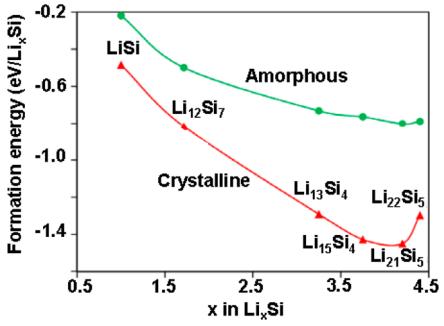

Figure 2. Calculated formation energy of Li_xSi in crystalline and amorphous forms.

electron microscopy,[36] *in situ* X-ray diffraction (XRD),[37] *ex situ* XRD,[38] *in situ* transmission electron microscopy (TEM),[15,25,39] and real-time nuclear magnetic resonance.[40] It is widely accepted that highly lithiated a-Li_xSi crystallizes "quickly" and exclusively to either $Li_{15}Si_4$ or $Li_{22}Si_5$.[15,39,41,42] However, the detailed atomistic mechanism is not fully understood. If the phase transformation happens according to the classic nucleation and growth model, one might expect composition fluctuations and phase separation in the amorphous phase that could adversely impact the stability of the material during charge/discharge.[41,42] *In situ* S/TEM observation provides a unique opportunity to reveal the fine details of such complex phase transformations. In this paper, we use *in situ* S/TEM and electron energy loss spectroscopy (EELS) to probe the structural and chemical evolution and phase transformation mechanisms of the electrochemically driven lithiation of silicon. In addition, DFT calculations establish that amorphous Li_xSi crystallizes to $Li_{15}Si_4$ through a spontaneous, congruent process without long distance displacement and diffusion of the atoms. This mechanism is drastically different from what is expected from the classic nucleation and growth process, which necessitates the involvement of long-range atomic diffusion or phase separation.

RESULTS AND DISCUSSION

The lithiation behavior and microstructural features of a single crystalline silicon nanowire are illustrated in

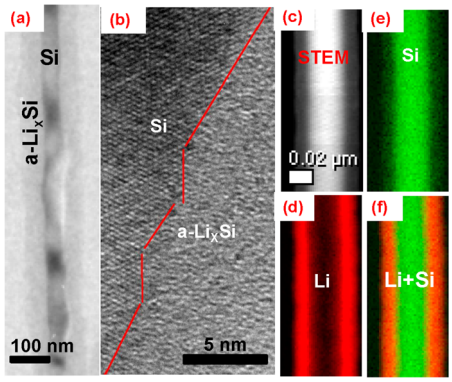

Figure 3. General microstructual features of the lithiated core–shell nanowire. (a) TEM image of Si core cladded with an a-Li_xSi shell. (b) Atomically resolved TEM image of the atomically abrupt and faceted a-Li_xSi/Si interface. (c) STEM image showing the Si core and a-Li_xSi shell. (d) Li distribution by EELS mapping. (e) Si distribution by EELS maping. (f) Superposed Li and Si distribution.

Figure 3. It has been very well documented in literature that the lithiation of silicon nanowire occurs through the formation of a-Li_xSi shell and Si core structure. This is clearly illustrated by the TEM image of Figure 3a, where the silicon core is revealed by the diffraction contrast. The lithiated shell is amorphous Li_xSi. The core–shell structure is demonstrated by the scanning transmission electron microscopy (STEM) high-angle annular dark-field (HAADF) image and the corresponding STEM-EELS elemental mapping shown in Figure 3c–f. As illustrated in Figure 3b, HRTEM image reveals that the interface between a-Li_xSi and Si is atomically abrupt. Recent literature indicates that the lithiation speed of silicon is controlled by the reaction rate of the lithium ion across the interface between the a-Li_xSi and Si;[43] the core–shell structure arises because the diffusion of Li at the surface of the nanowire is fast compared to the interfacial reaction.

Upon lithiation, the microstructure evolution of the silicon nanowire can be summarized with the following five features. (1) The lithium ion diffuses along the surface of the silicon nanowire, leading to a high concentration of lithium at the surface layer of the silicon nanowire. (2) The lithiation initiates from the surface of the nanowire and proceeds toward the core of the silicon nanowire, featuring the propagation of a boundary between the a-Li_xSi and Si crystalline as previously reported.[1] (3) Accompanying the conversion of Si to a-Li_xSi is a significant volume increase, which is accommodated by expansion along the radial direction. (4) As lithiation progresses, the lithiation rate decreases, as the silicon nanowire always retains a residual core even following a prolonged period of lithiation. This feature is similar to the lithiation behavior of crystalline silicon nanoparticles.[24,44] Detailed experimental and theoretical analyses have indicated that the lithation of Si is an interface reaction-controlled process, which normally yields to a constant

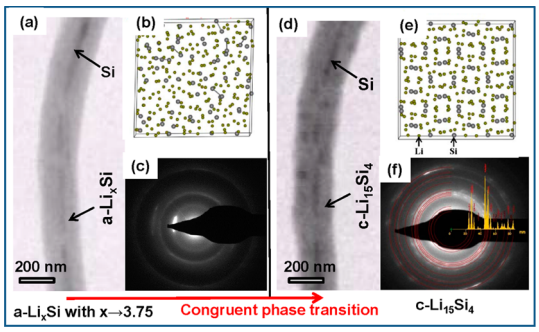

Figure 4. STEM bright-field image sequence revealing the spontaneous crystallization of a-Li$_x$Si to c-Li$_{15}$Si$_4$ when x reaches the critical value of 3.75. (a) STEM bright-field image of a-Li$_x$Si nanowire with residual silicon core in some sections. (b) Atomic arrangement in a-Li$_{3.75}$Si. (c) Electron diffraction pattern of a-Li$_x$Si. (d) STEM bright-field image showing the polycrystalline c-Li$_{15}$Si$_4$. (e) Atomic arrangement in c-Li$_{15}$Si$_4$. (f) Electron diffraction pattern of c-Li$_{15}$Si$_4$.

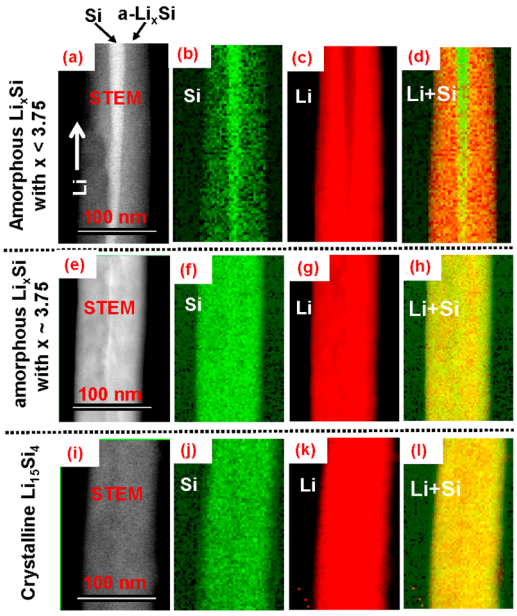

Figure 5. STEM annular dark-field image and EELS elemental distribution maps showing the congruent phase transition characteristics of the a-Li$_{3.75}$Si to c-Li$_{15}$Si$_4$. (a–d) Progression of the lithiation from bottom to top. (e–h) As x approaches 3.75 in a-Li$_x$Si. (i–l) Following the crystallization of a-Li$_x$Si to c-Li$_{15}$Si$_4$.

lithiation rate.[24,44,45] However, the stress field due to the large volume expansion reduces the lithation rate of crystalline silicon nanoparticles.[25,36,44–46] One may expect a similar effect in silicon nanowires. (5) Continued lithiation leads to an increase in the Li concentration in the a-Li$_x$Si. With a continuous increase in x, a-Li$_x$Si reaches a composition that could lead to a stoichiometric crystalline phase as illustrated in the phase diagram of Figure 1. However, it remains amorphous until x reaches a critical value of 3.75, at which point the a-Li$_x$Si crystallizes to Li$_{15}$Si$_4$, as clearly identified by the STEM bright-field image and electron diffraction analysis shown in Figure 4. The Li$_{15}$Si$_4$ is polycrystalline with a typical grain size of several tens of nanometers as visible by the dark contrast of the STEM bright-field image in Figure 4d. The transformation of a-Li$_x$Si to c-Li$_{15}$Si$_4$ has also been observed in other forms of silicon.[39,41,42] Therefore, in terms of lithiation-induced formation of a-Li$_x$Si and subsequent crystallization of a-Li$_x$Si to c-Li$_{15}$Si$_4$, there are no significant differences between amorphous and crystalline silicon as a starting material. One important difference is that the volume expansion for crystalline Si to a-Li$_x$Si is strongly anisotropic while the volume expansion for amorphous Si to a-Li$_x$Si is isotropic.

The crystallization of c-Li$_{15}$Si$_4$ from a-Li$_x$Si does not lead to phase segregation nor residual phase formation, indicating that the critical composition for this phase transformation is x = 3.75, as illustrated by the STEM images and STEM-EELS elemental mapping in Figure 5. Figure 5a–d reveals that the lithiated a-Li$_x$Si shell (for x < 3.75) on the unlithiated silicon core is compositionally uniform and contains no crystalline phases. This remains true as x approaches 3.75 (Figure 5e–h). With further lithiation (Figure 5i–l), the whole nanowire spontaneously transforms to crystalline Li$_{15}$Si$_4$ and shows no chemical composition fluctuations. The crystallization occurs through the fast propagation of the interface between the crystallized region and the amorphous region (crystallization front sweeping) along the Li$^+$ diffusion direction, indicating that the Li enrichment is achieved through the electrochemically driven Li$^+$ diffusion.

As is clear from the analysis above, the crystallization of Li$_{15}$Si$_4$ from a-Li$_{3.75}$Si is a congruent process in which the chemical composition is constant. As such, the transformation does not require long-range diffusion of the chemical species, but simply local rearrangement of atomic configurations.[47,48] The crystallization is initiated by electrochemically driven directional Li diffusion rather than random composition fluctuations resulting from the random walk of Li atoms. This crystallization process is termed "electrochemically driven congruent crystallization", which is the reverse process of electrochemically driven solid-state amorphization[1] and is drastically different from the classic nucleation and growth process for which local chemical composition fluctuations lead to phase separation. Though the formation of c-Li$_{15}$Si$_4$ from a-Li$_x$Si has been reported,[3,42] the congruent of this phase transformation has not been previously recognized. No significant volume change has been observed accompanying the crystallization of a-Li$_x$Si to crystalline c-Li$_{15}$Si$_4$.

A critical question that needs to be answered is why the formation of Li$_{15}$Si$_4$ (x = 3.75 in a-Li$_x$Si) is not preceded by the formation of other stable compounds, because some compounds have a lower value of x, such as LiSi (x = 1), Li$_{12}$Si$_7$ (x = 1.71), Li$_7$Si$_3$ (x = 2.33), and Li$_{13}$Si$_4$ (x = 3.25), as shown in Figure 1. Our DFT simulation provides insight into this question. First, the formation energy of Li$_x$Si in both amorphous and

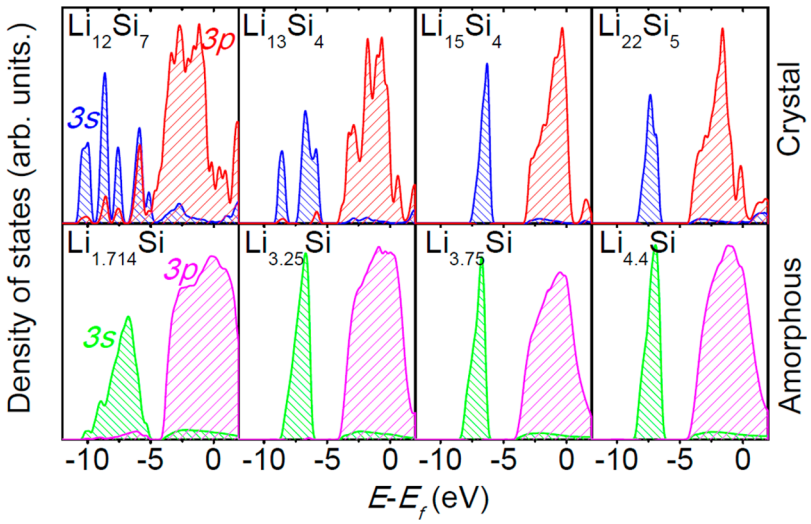

Figure 6. Density of states (DOS) projected on Si atoms in various crystalline and amorphous Li−Si alloys with the Fermi energy level set to zero.

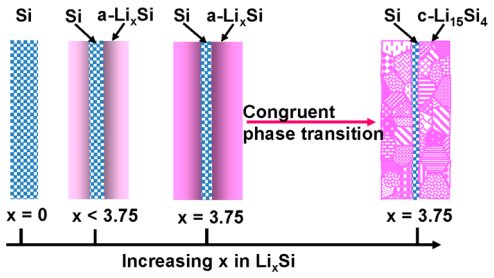

Figure 7. Schematic of the silicon nanowire lithiation process and the spontaneous congruent phase transition of a-Li_xSi to c-$Li_{15}Si_4$ when *x* reaches the critical value of 3.75 in the amorphous phase.

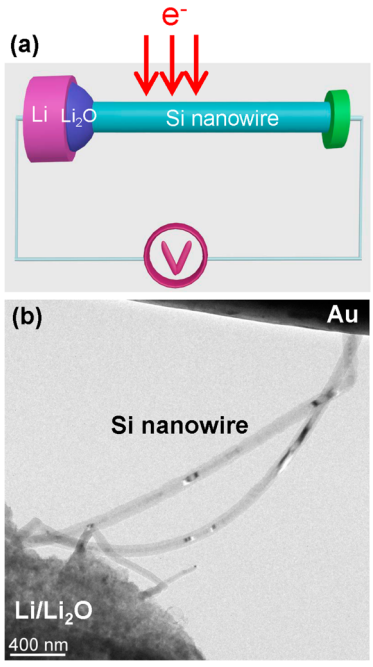

Figure 8. Nanobattery configuration used for *in situ* S/TEM study of the lithiation behavior of silicon nanowire. (a) Schematic drawing. (b) TEM image showing the connection of silicon nanowire and the Li/Li_2O under TEM observation.

crystalline forms is given by $E_{formation}(x) = E_{Li_xSi} - xE_{Li} - E_{Si}$, where *x* is the number of Li atoms per Si atom and $E_{formation}$ is the formation energy. E_{Li_xSi} is the total energy of the Li_nSi_m (such as $Li_{15}Si_4$) structure divided by the number of Si atoms; E_{Li} and E_{Si} are the energies of a Li atom in body-centered cubic Li and a Si atom in a diamond structure, respectively. The values of $E_{formation}$, E_{Li_xSi}, E_{Li}, and E_{Si} are shown in Table S1 in the Supporting Information. The formation energies of amorphous Li_xSi alloys are higher than those of the crystalline ones (Figure 2), and it is evident that crystalline $Li_{15}Si_4$ and $Li_{21}Si_5$ have the lowest formation energies, which means that, thermodynamically, crystalline intermetallics of Li_xSi have much lower Gibbs energy than the amorphous alloys. This result demonstrates well that a range of solid crystalline compounds can be formed, including LiSi, $Li_{12}Si_7$, $Li_{13}Si_4$, and $Li_{22}Si_5$, through thermal treatment of a mixture of Li and Si. Second, we also calculated the density of states (DOS) projected on Si atoms in the crystalline and amorphous Li−Si alloys as shown in Figure 6. The Fermi energy level (E_f) is set to zero, which is used as a reference. For crystalline Li−Si alloys, the splitting between the 3s and 3p states grows larger as the Li concentration increases to 4.4 ($Li_{22}Si_5$) per Si. This is because, with increasing Li concentration, Si frameworks show a decrease in connectivity with typically three-fold-coordinated Si ions forming interconnected chains and puckered with eight-membered rings in LiSi; 5-Si-rings and 4-Si-'Y' (three-pointed planar Si4 stars) in $Li_{12}Si_7$; Si_2 dumbbells in $Li_{3.25}Si$; and isolated Si in both $Li_{3.75}Si$ and $Li_{4.4}Si$. With the decrease of the Si connectivity, the Si−Si interaction decreases, thus weakening the s−p hybridization. For both crystalline and amorphous alloys, the distribution of the 3s and 3p states becomes narrower with increasing Li,

which is attributed to the decrease in the Si−Si bond interactions and the weakened s−p hybridization. The salient feature of the system is the increasing similarity of the electronic structure's amorphous and crystalline phases as x approaches the critical value of 3.75. This result is consistent with prior results that, at sufficiently high x, a-Li_xM (M = Si and Ge) shows chemical properties similar to those of crystalline $Li_{15}M_4$.[3,37,39,42,49−51] Overall, the lithiation, microstructural evolution, and the congruent phase transition characteristics of lithiated silicon are schematically illustrated in Figure 7.

The congruent phase transformation of a-$Li_{3.75}Si$ to c-$Li_{15}Si_4$ does not involve large-scale atomic motion. However, it does involve local bonding configuration changes. The grain size of the crystalline phase provides a characteristic length scale at which the atomic bonding configuration has been changed within a short time period. More work involving microscopy and spectroscopy with high spatial and fast temporal resolution is needed to capture the local atomic rearrangement process during the congruent phase transition.

CONCLUSIONS

The present observation correlates microstructure, phase, chemical composition, and phase transition characteristics during the lithiation of crystalline silicon. With increasing lithium concentration in the a-Li_xSi, the a-Li_xSi transforms to crystalline $Li_{15}Si_4$. Crystallization of $Li_{15}Si_4$ from a-Li_xSi is a congruent process that does not require long-range atomic diffusion nor any phase separation. As x increases, the electronic structure of a-Li_xSi approaches that of the crystalline phase of the same chemical composition. This accounts for the formation of $Li_{15}Si_4$ rather than other crystalline compounds.

METHODS

The *in situ* TEM testing was carried out using a nanobattery configuration with a single silicon chemical vapor deposition grown nanowire as the anode, Li as cathode, and Li_2O as a solid electrolyte as reported previously and illustrated in Figure 8.[52] All the *in situ* electrochemical tests were conducted on a Titan 80-300 kV S/TEM operated at 300 kV. Assembly of the nanobattery was conducted in an Ar-filled glovebox, and the entire assembly was transferred to the microscope column within a sealed plastic bag. The lithium metal was only exposed to air during the insertion of the TEM holder into the microscope column, which is typically about 2 s. During this short period of air exposure, the surface of the lithium metal was oxidized to Li_2O, which acts as the solid electrolyte for the function of the nanobattery. During the lithiation of the silicon, zero potential was applied. The spatial distribution of chemical composition during the lithiation was mapped *in situ* using S/TEM EELS. The STEM EELS was carried out using a Gatan Image Filter (Quantum 965) that is post-column-attached to the Titan S/TEM. The energy resolution of the EELS spectrometer is ~0.9 eV as measured by the full width at half-magnitude of the zero loss peak. The typical dwell time for each pixel is ~1−5 ms. To minimize artifacts related to sample drift during the STEM EELS mapping, the mapping is drift corrected every 30 pixels. The integration window is 55−85 eV for the Li K edge and 99−170 eV for the Si L edge. In the processing of the EELS maps, the variation of the thickness across the radial direction of the nanowire is not quantitatively considered. Due to the small diameter of the Si nanowire, the thickness variation of the nanowire doesn't seem to impact the EELS signal dramatically. Therefore, the contrast in the EELS maps is dominated by the elemental concentrations.

All the calculations were performed using density functional theory, within the local density approximation[53] using the Ceperly−Alder parametrization as implemented in the SIESTA code,[54] which adopts a linear combination of numerical localized atomic orbital basis sets for the description of valence electrons and norm-conserving nonlocal pseudopotentials for the atomic core.[55] The valence electron wave functions were expanded by using double-ζ basis set. The charge density was projected on a real space grid with a cutoff of 120 Ry to calculate the self-consistent Hamiltonian matrix elements. The crystalline alloys were constructed from the crystalline structure database and experimental results. The amorphous structures were prepared by using the melt quenching method with density functional theory molecular dynamics simulations. We equilibrated the system at a temperature of 4000 K at least for 5 ps (5000 MD steps with a time step of 1 fs), which is above the melting point. We then quickly quenched the systems to ~0 K, and the lattices were further relaxed together with the atomic coordinates using the conjugate gradient minimization. Large systems were used to model the amorphous structures. The numbers of atoms used for the $E_{Li,Si}$ alloys are as follows: LiSi (192/192), $Li_{12}Si_7$ (192/112), $Li_{13}Si_4$ (208/64), $Li_{15}Si_4$ (240/64), $Li_{21}Si_5$ (336/80), and $Li_{22}Si_5$ (352/80).

Conflict of Interest: The authors declare no competing financial interest.

Acknowledgment. The research described in this paper is part of the Chemical Imaging Initiative at Pacific Northwest National Laboratory (PNNL). It was conducted under the Laboratory Directed Research and Development Program at PNNL, a multiprogram national laboratory operated by Battelle under Contract DE-AC05-76RLO1830 for the U.S. Department of Energy (DOE). The work was conducted in the William R. Wiley Environmental Molecular Sciences Laboratory (EMSL), a national scientific user facility sponsored by DOE's Office of Biological and Environmental Research and located at PNNL. Work at Northwestern University was supported by NSF DMR-1006069.

Supporting Information Available: Supporting movie showing the charging of the silicon nanowire and the particles loaded on the silicon nanowire and the tabled specific parameters used in the DFT calculation. This material is available free of charge *via* the Internet at http://pubs.acs.org.

REFERENCES AND NOTES

1. Limthongkul, P.; Jang, Y. I.; Dudney, N. J.; Chiang, Y. M. Electrochemically-Driven Solid-State Amorphization in Lithium-Silicon Alloys and Implications for Lithium Storage. *Acta Mater.* **2003**, *51*, 1103–1113.
2. Lee, S. W.; McDowell, M. T.; Choi, J. W.; Cui, Y. Anomalous Shape Changes of Silicon Nanopillars by Electrochemical Lithiation. *Nano Lett.* **2011**, *11*, 3034–3039.
3. Liu, X. H.; Zheng, H.; Zhong, L.; Huang, S.; Karki, K.; Zhang, L. Q.; Liu, Y.; Kushima, A.; Liang, W. T.; Wang, J. W.; *et al.* Anisotropic Swelling and Fracture of Silicon Nanowires during Lithiation. *Nano Lett.* **2011**, *11*, 3312–3318.
4. Boukamp, B. A.; Lesh, G. C.; Huggins, R. A. All-Solid Lithium Electrodes with Mixed-Conductor Matrix. *J. Electrochem. Soc.* **1981**, *128*, 725–729.
5. Larcher, D.; Beattie, S.; Morcrette, M.; Edstroem, K.; Jumas, J. C.; Tarascon, J. M. Recent Findings and Prospects in the Field of Pure Metals as Negative Electrodes for Li-Ion Batteries. *J. Mater. Chem.* **2007**, *17*, 3759–3772.
6. Chan, C. K.; Peng, H.; Liu, G.; McIlwrath, K.; Zhang, X. F.; Huggins, R. A.; Cui, Y. High-Performance Lithium Battery Anodes Using Silicon Nanowires. *Nat. Nanotechnol.* **2007**, *3*, 31–35.

7. Park, M. H.; Kim, M. G.; Joo, J.; Kim, K.; Kim, J.; Ahn, S.; Cui, Y.; Cho, J. Silicon Nanotube Battery Anodes. *Nano Lett.* **2009**, *9*, 3844–3847.
8. Song, T.; Xia, J. L.; Lee, J. H.; Lee, D. H.; Kwon, M. S.; Choi, J. M.; Wu, J.; Doo, S. K.; Chang, H.; Park, W. I.; *et al.* Arrays of Sealed Silicon Nanotubes as Anodes for Lithium Ion Batteries. *Nano Lett.* **2010**, *10*, 1710–1716.
9. Cui, L.-F.; Hu, L. B.; Choi, J. W.; Cui, Y. Light-Weight Free-Standing Carbon Nanotube-Silicon Films for Anodes of Lithium Ion Batteries. *ACS Nano* **2010**, *4*, 3671–3678.
10. Cho, J. Porous Si Anode Materials for Lithium Rechargeable Batteries. *J. Mater. Chem.* **2010**, *20*, 4009–4014.
11. Kim, H.; Han, B.; Choo, J.; Cho, J. Three-Dimensional Porous Silicon Particles for Use in High-Performance Lithium Secondary Batteries. *Angew. Chem., Int. Ed.* **2008**, *47*, 10151–10154.
12. Zhang, J. G.; Liu, J.; Wang, D. H.; Choi, D.; Fifield, L. S.; Wang, C. M.; Xia, G.; Nie, Z. M.; Yang, Z. G.; Pederson, L. R.; *et al.* Vapor-Induced Solid–Liquid–Solid Process for Silicon-Based Nanowire Growth. *J. Power Sources* **2010**, *195*, 1691.
13. Magasinski, A.; Dixon, P.; Hertzberg, B.; Kvit, A.; Ayala, J.; Yushin, G. High-Performance Lithium-Ion Anodes Using a Hierarchical Bottom-up Approach. *Nat. Mater.* **2010**, *9*, 353–358.
14. Zhou, S.; Liu, X. H.; Wang, D. W. Si/$TiSi_2$ Hetero-Nanostructures as High-Capacity Anode Material for Li Ion Batteries. *Nano Lett.* **2010**, *10*, 860–863.
15. Ghassemi, H.; Au, M.; Chen, N.; Heiden, P. A.; Yassar, R. S. *In Situ* Electrochemical Lithiation/Delithiation Observation of Individual Amorphous Si Nanorods. *ACS Nano* **2011**, *5*, 7805–7811.
16. Cui, L. F.; Yang, Y.; Hsu, C. M.; Cui, Y. Carbon-Silicon Core–Shell Nanowires as High Capacity Electrode for Lithium Ion Batteries. *Nano Lett.* **2009**, *9*, 3370–3374.
17. Wang, W.; Kumta, P. N. Nanostructured Hybrid Silicon/Carbon Nanotube Heterostructures: Reversible High-Capacity Lithium-Ion Anodes. *ACS Nano* **2010**, *4*, 2233–2241.
18. Hu, L.; Wu, H.; Gao, Y.; Cao, A.; Li, H.; McDough, J.; Xie, X.; Zhou, M.; Cui, Y. Silicon-Carbon Nanotube Coaxial Sponge as Li-Ion Anodes with High Areal Capacity. *Adv. Energy Mater.* **2011**, *1*, 523–527.
19. Ng, S. H.; Wang, J.; Wexler, D.; Chew, S. Y.; Liu, H. K. Amorphous Carbon-Coated Silicon Nanocomposites: A Low-Temperature Synthesis *via* Spray Pyrolysis and Their Application as High-Capacity Anodes for Lithium-Ion Batteries. *J. Phys. Chem. C* **2007**, *111*, 11131–11138.
20. Yang, J.; Wang, B. F.; Wang, K.; Liu, Y.; Xie, J. Y.; Wen, Z. S. Si/C Composites for High Capacity Lithium Storage Materials. *Electrochem. Solid State* **2003**, *6*, A154–A156.
21. Xue, J. S.; Myrtle, K.; Dahn, J. R. An Epoxy-Silane Approach To Prepare Anode Materials for Rechargeable Lithium Ion Batteries. *J. Electrochem. Soc.* **1995**, *142*, 2927–2935.
22. Jang, S. M.; Miyawaki, J.; Tsuji, M.; Mochida, I.; Yoon, S. H. The Preparation of a Novel Si-CNF Composite as an Effective Anodic Material for Lithium-Ion Batteries. *Carbon* **2009**, *47*, 3383–3391.
23. Cui, L. F.; Ruffo, R.; Chan, C. K.; Peng, H. L.; Cui, Y. Crystalline-Amorphous Core–Shell Silicon Nanowires for High Capacity and High Current Battery Electrodes. *Nano Lett.* **2009**, *9*, 491–495.
24. Gu, M.; Li, Y.; Li, X. L.; Hu, S. Y.; Zhang, X.; Xu, W.; Thevuthasan, S.; Baer, D. R.; Zhang, J. G.; Liu, J.; *et al. In Situ* TEM Study of Lithiation Behavior of Silicon Nanoparticles Attached to and Embedded in a Carbon Matrix. *ACS Nano* **2012**, *6*, 8439–8447.
25. Wang, C.-M.; Li, X.; Wang, Z.; Xu, W.; Liu, J.; Gao, F.; Kovarik, L.; Zhang, J.-G.; Howe, J.; Burton, D. J.; *et al. In-Situ* TEM Investigation of Congruent Phase Transition and Structural Evolution of Nanostructured Silicon/Carbon Anode for Lithium Ion Batteries. *Nano Lett.* **2012**, *12*, 1624–1632.
26. Liu, N.; Wu, H.; McDowell, M. T.; Yao, Y.; Wang, C. M.; Cui, Y. A Yolk-Shell Design for Stabilized and Scalable Li-Ion Battery Alloy Anodes. *Nano Lett.* **2012**, *12*, 3315–3321.
27. Kim, H.; Kweon, K. E.; Chou, C. Y.; Ekerdt, J. G.; Hwang, G. S. On the Nature and Behavior of Li Atoms in Si: A First Principles Study. *J. Phys. Chem. C* **2010**, *114*, 17942–17946.
28. Kim, H.; Chou, C. Y.; Ekerdt, J. G.; Hwang, G. S. Structure and Properties of Li-Si Alloys: A First-Principles Study. *J. Phys. Chem. C* **2011**, *115*, 2514–2521.
29. Chou, C. Y.; Kim, H.; Hwang, G. S. A Comparative First-Principles Study of the Structure, Energetics, and Properties of Li-M (M = Si, Ge, Sn) Alloys. *J. Phys. Chem. C* **2011**, *115*, 20018–20026.
30. Zhang, Q. F.; Zhang, W. X.; Wan, W. H.; Cui, Y.; Wang, E. G. Lithium Insertion in Silicon Nanowires: An *Ab Initio* Study. *Nano Lett.* **2010**, *10*, 3243–3249.
31. Zhang, Q. F.; Cui, Y.; Wang, E. G. Anisotropic Lithium Insertion Behavior in Silicon Nanowires: Binding Energy, Diffusion Barrier, and Strain Effect. *J. Phys. Chem. C* **2011**, *115*, 9376–9381.
32. Zhao, K. J.; Wang, W. L.; Gregoire, J.; Pharr, M.; Suo, Z. G.; Vlassak, J. J.; Kaxiras, E. Lithium-Assisted Plastic Deformation of Silicon Electrodes in Lithium-Ion Batteries: A First-Principles Theoretical Study. *Nano Lett.* **2011**, *11*, 2962–2967.
33. Okamoto, H. Li-Si (Lithium-Silicon). *J. Phase Equilib. Diffus.* **2009**, *30*, 118–119.
34. Okamoto, H. The Li-Si (Lithium-Silicon) System. *Bull. Alloy Phase Diagrams* **1990**, *11*, 306–312.
35. van der Marel, C.; Vinke, G. J. B.; van der Lugt, W. The Phase Diagram of the System Lithium-Silicon. *Solid State Commun.* **1985**, *54*, 917–919.
36. Chon, M. J.; Sethuraman, V. A.; McCormick, A.; Srinivasan, V.; Guduru, P. R. Real-Time Measurement of Stress and Damage Evolution during Initial Lithiation of Crystalline Silicon. *Phys. Rev. Lett.* **2011**, *107*, 045503.
37. Hatchard, T. D.; Dahn, J. R. *In-Situ* XRD and Electrochemical Study of the Reaction of Lithium with Amorphous Silicon. *J. Electrochem. Soc.* **2004**, *151*, A838–A842.
38. Li, H.; Huang, X.; Chen, L.; Zhou, G.; Zhang, Z.; Yu, D.; Jun, M. Y.; Pei, N. The Crystal Structural Evolution of Nano-Si Anode Caused by Lithium Insertion and Extraction at Room Temperature. *Solid State Ionics* **2000**, *135*, 181–191.
39. Liu, X. H.; Zhang, L. Q.; Zhong, L.; Liu, Y.; Zheng, H.; Wang, J. W.; Cho, J. H.; Dayeh, S. A.; Picraux, S. T.; Sullivan, J. P.; *et al.* Ultrafast Electrochemical Lithiation of Individual Si Nanowire Anodes. *Nano Lett.* **2011**, *11*, 2251–2258.
40. Key, B.; Bhattacharyya, R.; Morcrette, M.; Seznec, V.; Tarascon, J. M.; Grey, C. P. Real-Time NMR Investigations of Structural Changes in Silicon Electrodes for Lithium-Ion Batteries. *J. Am. Chem. Soc.* **2009**, *131*, 9239–9249.
41. Li, J.; Dahn, J. R. An *In-Situ* X-ray Dirraction Study of the Reaction of Li with Crystalline Si. *J. Electrochem. Soc.* **2007**, *154*, A156–A161.
42. Obrovac, M. N.; Christensen, L. Structural Changes in Silicon Anodes during Lithium Insertion/Extraction. *Electrochem. Solid State Lett.* **2004**, *7*, A93–A96.
43. Yang, H.; Huang, S.; Huang, X.; Fan, F.; Liang, W.; Liu, X. H.; Chen, L.-Q.; Huang, J. Y.; Li, J.; Zhu, T.; *et al.* Orientation-Dependent Interfacial Mobility Governs the Anisotropic Swelling in Lithiated Silicon Nanowires. *Nano Lett.* **2012**, *12*, 1953–1958.
44. McDowell, M. T.; Ryu, I.; Lee, S. W.; Wang, C. M.; Nix, W. D.; Cui, Y. Studying the Kinetics of Crystalline Silicon Nanoparticle Lithiation with *In Situ* Transmission Electron Microscopy. *Adv. Mater.* **2012**, *24*, 6034–6041.
45. Zhao, K. J.; Pharr, M.; Wan, Q.; Wang, W. L.; Kaxiras, E.; Vlassak, J. J.; Suo, Z. G. Concurrent Reaction and Plasticity during Initial Lithiation of Crystalline Silicon in Lithium-Ion Batteries. *J. Electrochem. Soc.* **2012**, *159*, A238–A243.
46. Deshpande, R.; Cheng, Y.-T.; Verbrugge, M. W.; Timmons, A. Diffusion Induced Stresses and Strain Energy in a Phase-Transforming Spherical Electrode Particle. *J. Electrochem. Soc.* **2011**, *158*, A718–A724.
47. Zubarev, E. N. Reactive Diffusion in Multilayer Metal/Silicon Nanostructures. *Phys.-Usp.* **2011**, *54*, 473–498.
48. Gonzalez-Hernandez, J.; Chao, B. S.; Strand, D.; Ovshinsky, S. R.; Pawlik, D.; Gasionrowski, P. The Relationship between Crystal Structure and Performance as 58 Optical Recording Media in Te-Ge-Sb Thin Films. *Appl. Phys. Commun.* **1992**, *11*, 557–581.

49. Johnson, Q.; Smith, G. S.; Wood, D. The Crystal Structure of $Li_{15}Ge_4$. *Acta Crystallogr.* **1965**, *18*, 131–132.
50. Obrovac, M. N.; Krause, L. J. Reversible Cycling of Crystalline Silicon Powder. *J. Electrochem. Soc.* **2007**, *154*, A103–A108.
51. Liang, W.; Yang, H.; Fan, F.; Liu, Y.; Liu, X. H.; Huang, J. Y.; Zhu, T.; Zhang, S. Tough Germanium Nanoparticles under Electrochemical Cycling. *ACS Nano* **2013**, *7*, 3427–3433.
52. Liu, X. H.; Huang, S.; Picraux, S. T.; Li, J.; Zhu, T.; Huang, J. Y. Reversible Nanopore Formation in Ge Nanowires during Lithiation–Delithiation Cycling: An *In Situ* Transmission Electron Microscopy Study. *Nano Lett.* **2011**, *11*, 3991–3997.
53. Ceperley, D. M.; Alder, B. J. Ground State of the Electron Gas by a Stochastic Method. *Phys. Rev. Lett.* **1980**, *45*, 566–569.
54. Soler, J. M.; Artacho, E.; Gale, J. D.; Garcia, A.; Junquera, J.; Ordejon, P.; Sanchez-Portal, D. The Siesta Method for *Ab Initio* Order-N Materials Simulation. *J. Phys.: Condens. Matter* **2002**, *14*, 2745.
55. Troullier, N.; Martins, J. L. Efficient Pseudopotentials for Plane-Wave Calculations. *Phys. Rev. B* **1991**, *43*, 1993–2006.